Application of a new scheme of cloud base droplet nucleation in a Spectral (bin) Microphysics cloud model: sensitivity to aerosol size distribution

E. Ilotoviz and A. Khain

Department of Atmospheric Sciences, The Hebrew University of Jerusalem, Israel

Submitted to Atmos. Chem. Phys. Discuss.

June 2016

Revised

21 September 2016

Communicating author: Alexander Khain, Department of Atmospheric Sciences, The Hebrew University of Jerusalem, Israel, email: alexander.khain@mail.huji.ac.il

Abstract

A new scheme of droplet nucleation at cloud base is implemented into the Hebrew University Cloud Model (HUCM) with spectral (bin) microphysics. In this scheme, supersaturation maximum S_{max} near cloud base is calculated using theoretical results according to which $S_{\max} \sim w^{3/4} N_d^{-1/2}$, where w is the vertical velocity at cloud base and N_d is droplet concentration. Microphysical cloud structure obtained in the simulations of a mid-latitude hail storm using the new scheme is compared with that obtained in the standard approach, in which droplet nucleation is calculated using supersaturation calculated in grid points. The simulations were performed with different concentrations of cloud condensational nuclei (CCN) and with different shapes of CCN size spectra. It is shown that the new nucleation scheme substantially improves the vertical profile of droplet concentration shifting the concentration maximum to cloud base. It is shown that the effect of the CCN size distribution shape on cloud microphysics is not less important that the effect of the total CCN concentration. It is shown that the smallest CCN with diameters less than about 0.015 μm have a substantial effect on mixed-phase and ice microphysics of deep convective clouds. Such CCN are not measured by standard CCN probes which hinders understanding of cold microphysical processes.

Key words: cloud-aerosol interaction, droplet nucleation at cloud base, spectral bin microphysics

1. Introduction

Droplet concentration is the key microphysical parameter that affects precipitation formation, and radiative cloud properties (Pruppacher and Klett, 1997). The droplet concentration determines major microphysical cloud properties such as height of precipitation onset, type of precipitation (liquid, mixed phase and ice) (Khain, 2009; Freud and Rosenfeld, 2012; Tao et al. 2012) . Droplet concentration is determined by concentration and size distribution of aerosol particles (AP) and by the maximum value of supersaturation near cloud base $S_{\max}$. $S_{\max}$ is reached at a few tens of meters above cloud base (Rogers and Yau, 1996). The vertical grid spacing of most cloud-resolving models is too coarse to resolve this maximum. This can lead to errors in determination of droplet concentration. Therefore, it is desirable to parameterize the process of droplet nucleation near cloud base. One approach to the parameterization is based on lookup tables developed using precise 1D parcel models (e.g., Segal and Khain, 2006). The other approach is based on analytical calculation of supersaturation maximum, $S_{\max}$, near cloud base. This approach has been developed in several studies using various assumptions concerning CCN activity spectra (Ghan et al., 1993, 1997; Bedos et al., 1996; Abdul-Razzak et al., 1998; Cohard et al., 1998; Abdul-Razzak and Ghan, 2000; Fountoukis, 2005; Shipway and Abel, 2010). In these studies calculation of a supersaturation maximum is reduced to solving a complicated integro-differential equation assuming different expressions for CCN activation spectra. The parameters of activation CCN spectra, as well as the concentration and shape of the CCN size distributions, are often prescribed in atmospheric models and assumed to be invariant over time. The results and a comparison of these approaches are presented by Ghan et al. (2011).

In cloud models with a comparatively high resolution (Kogan 2001; Khain et al. 2014) supersaturation S_w is calculated explicitly at each grid point. In these bin microphysics models AP playing the role of cloud condensational nuclei (CCN) are described using aerosol size distribution functions containing several tens of size bins. The value of supersaturation is used to calculate the critical radius of AP using the Köhler theory. All CCN with sizes exceeding this critical value are activated to droplets. This approach will be referred to as standard approach (ST) where supersaturation maximum near cloud base is not resolved and the vertical profile of supersaturation may not contain such maximum. It leads to underestimation of droplet concentration in clouds, at least in their low part.

In set of studies by Pinsky et al. (2012, 2013, 2014) formation of profiles of supersaturation and of droplet concentration were investigated both analytically and by means of a high precision model of an ascending adiabatic parcel. Pinsky et al. (2012) proposed a simple method of calculating $S_{\max}$ near cloud base for monodisperse aerosol size distribution. The detailed test showed that the method can be applied to any CCN spectra. Pinsky et al (2014) gave a theoretical basis for such conclusion by calculating droplet concentrations using multidisperse size spectra of AP. The method of calculating droplet concentration near cloud base using $S_{\max}$ will be referred to as *new approach* (NA).

In this study we investigate the effects of application of NA on the microphysics of mid-latitude deep convective clouds (hail storm) using the Hebrew University Cloud model (HUCM) with spectral-bin microphysics (SBM). The effect of the new approach is investigated in simulations with different parameters of CCN activation spectra.

2. Model description

The HUCM is a 2-D, nonhydrostatic SBM model with microphysics based on solving a system of equations for size distributions of liquid drops, three types of pristine ice crystals (plates, columns, and dendrites), snow/aggregates, graupel, hail and partially frozen or "freezing drops". Each size distribution is discretized into 43 mass-doubling bins, with the smallest bin equivalent to the mass of a liquid droplet of radius 2 μm. AP playing the role of CCN are also defined on a mass grid containing 43 mass bins. The size of dry CCNs ranges from 0.005 μm to 2 μm.

Primary nucleation of each ice crystal type is described using Meyers et al. [1992] parameterization. The type of ice crystals is determined depending on temperature range where the particles arise (Takahashi et al., 1991). Secondary ice generation is taken into account during riming (Hallett and Mossop 1974). Collisions are described by solving the stochastic collection equations for the corresponding size distributions using the Bott (1998) method. Height-dependent, gravitational collision kernels for drop-drop and drop-graupel interactions are taken from Pinsky et al. (2001) and Khain et al. (2001); those for collisions between ice crystals are taken from Khain and Sednev (1995) and Khain et al. (2004). The latter studies include the dependence of particle mass on the ice crystal cross-section. The effects of turbulence on collisions between cloud drops are included (Benmoshe et al. 2012). The collision kernels depend on the turbulence intensity and changes over time and space.

The time-dependent melting of snow, graupel, and hail as well as shedding of water from hail follows the approach suggested by Phillips et al. (2007). We have implemented liquid water mass in these hydrometeor particles that is advected and settle similarly to the mass of the corresponding particles. As a result, these particles are characterized by their total mass and by the

mass of liquid water (i.e., the liquid water mass fraction). The liquid water fraction increases during melting. As soon as it exceeds ~95%, the melting particles are converted to raindrops. Process of time dependent freezing is described according to Phillips et al. (2014, 2015). The freezing process consists of two stages. The first nucleation stage is described using the parameterization of immersion drop freezing proposed by Vali (1994) and Bigg (1953). Drops with radii below 80 μm that freeze are assigned to plates, whereas larger drops undergoing freezing are assigned to freezing drops. The freezing drops consist of a core of liquid water surrounded by an ice envelope. Time-dependent freezing of liquid within freezing drops is calculated by solving the heat balance equations that take into account the effects of accretion of supercooled drops and ice particles. Collision between freezing drops and other hydrometeors lead either to the freezing drops category if the freezing drop is larger than its counterpart. Otherwise, the resulting particle is assigned to the type of counterpart. Once the liquid water fraction in a freezing drop becomes less than some minimal value (<1%) it is converted to a hailstone. Hail can grow either by dry growth or by wet growth (Phillips et al. 2014, 2015). Accordingly, liquid water is allowed in hail and graupel particles at both positive and negative temperatures. The shedding of water in wet growth is also included.

Water accreted onto aggregates (snow) freezes immediately at temperatures below 0^0C, where it then contributes to the rimed fraction. This rimed mass distribution is advected and settle similarly to the snow masses. Riming mass increases the density of the aggregates. As the bulk density of snow in a certain mass bin exceeds a critical value (0.2 $g\ cm^{-3}$), the snow from this bin is converted into graupel. The appearance of water on the surface of hailstones as well as an increase in the rimed fraction of snowflakes affect the particle fall velocities and coalescence efficiencies.

The initial size distribution of CCN (at t=0) is calculated using the empirical dependence (i.e., the Twomey formula) of concentration N_{ccn} of activated CCN on supersaturation S_w (in %) $N_{ccn} = N_o S_w^k$, where N_o and k are the measured constants (Khain et al., 2000). The obtained aerosol size distribution is corrected in zones of very small and very large CCN, that is, in size ranges where the Twomey formula is invalid. At t>0 the prognostic equation for the size distribution of non-activated CCN is solved. Using the value of S calculated at each time-step and in each grid point, the critical radius of CCN particles was determined according to the Köhler theory. The CCNs with radii exceeding the critical value are activated and new droplets are nucleated. The corresponding bins of the CCN size distributions become empty. In ST, this procedure is used at all cloud grid points.

In NA, droplet concentration at cloud base is calculated using the formula for $S_{\max}$ derived by Pinsky et al. (2012)

$$S_{max} = Cw^{3/4} N_d^{-1/2}, \qquad (1)$$

where w is vertical velocity at cloud base, N_d is droplet concentration and coefficient C slightly depends on the thermodynamical parameters only (see **Table 1** for notations). A brief derivation of the formula (1) is presented in **Appendix**. Since the droplet concentration at cloud base is equal to the concentration of CCN activated at $S_w = S_{\max}$, the droplet concentration at the cloud base can be calculated as:

$$N_d = \int_{r_{n\_cr}(S_{\max})}^{\infty} f(r_n)\, dr_n \qquad (2)$$

where $f(r_n)$ is a size distribution of dry AP and r_{n_cr} is critical radius of CCN activated under $S_{\max}$. According to the Köhler theory, the critical radius relates to $S_{\max}$ as

$$r_{n\_cr} = \frac{A}{3}\left(\frac{4}{BS_{\max}^2}\right)^{1/3}, \qquad (3)$$

where coefficients A and B are the coefficients of the Köhler equation for equilibrium supersaturation (see Table 1 for notations). Substituting Eq. (2) into (1) one can obtain equation for $S_{\max}$:

$$S_{\max}\underbrace{\left[\int_{r_{n\_cr}(S_{\max})}^{\infty} f(r_n)\,dr_n\right]^{1/2}}_{N_d} = Cw^{3/4} \qquad (4)$$

Taking into account the relationship (3), Eq. (4) contains only one unknown $S_{\max}$. This equation is easily solved by iteration calculating $S_{\max}$, $r_{n\_cr}(S_{\max})$ and concentration of nucleated droplets at cloud base at each time step.

The values of $S_{\max}$ were calculated at all grid points corresponding to cloud base, which is determined as the first grid point from below, at which $S_w \geq 0$.

3. Design of simulations

All simulations were performed within a computational domain of 153.9 km x 19.2 km, and a grid spacing of 300 m in the horizontal direction and 100 m in the vertical direction. Effects of NA on cloud microphysics were tested in simulations of a thunderstorm observed in Villingen-Schwenningen, southwest Germany, on June 28, 2006**.** Meteorological conditions (including sounding) of this storm are described by Khain et al. [2011]. The background wind direction was

168 quasi-2-D, which simplified the prescription of the background wind profile in the 2-D model. The
169 wind speed increased with height from ~10 $m\,s^{-1}$ in the lower atmosphere to about 20 $m\,s^{-1}$ at
170 levels of 100-200 mb. Surface temperature was 22.9℃, the relative humidity near the ground was
171 high (~85%), which led to a low lifting condensation level of about 890 m. The freezing level was
172 located at around 3.5 km. The observed maximum diameter of hailstones was about 5 cm.
173 The convection was triggered by a cool pool, which is typical in simulations of long-lasting
174 convection (Rotunno and Klemp, 1985).
175 Three sets of simulations were performed, each simulation in two versions: according to ST
176 where the critical CCN radius was calculated using a supersaturation calculated at the grid points
177 using the values of temperature and humidity, and according to NA where the critical CCN radius
178 and $S_{\max}$ were determined from Eq. (9).

179 *The first set of simulations* aims at the comparison of the microphysics between NA and ST
180 in cases of high (N_0 =3500 cm^{-3}) and low (N_0 =100 cm^{-3}) CCN concentrations. Minimum
181 CCN radii were set equal to 0.015 μm and 0.0125 μm, respectively. These values correspond to
182 the data according to which the nuclei mode (the smallest CCN) in Marine aerosol size
183 distribution contains aerosols smaller than the nuclei mode in Continental case or even than in
184 Urban case (Ghan et al, 2011). Similar CCN size distributions were used by Khain et al (2011).
185 These simulations are referred to as E3500, E100 (T) and EN3500, EN100 (NA), respectively.
186 In *the second set of simulations* the smallest CCN were added into the AP spectra. The large
187 impact of the smallest CCN in formation of ice crystals in cloud anvils was shown by Khain et al.
188 (2012). The minimum CCN radii were taken equal to 0.006 μm and 0.003 μm in cases of high

and low CCN concentrations, respectively. These simulations are referred to as E3500-S, EN3500-S, E100-S and EN100-S, where symbol "S" denotes small AP.

In the first and the second sets of simulations the slope parameter k was assumed equal to 0.9.

The third set of simulations was similar to the second one, but with the slope parameter k =0.5. In many studies investigating effects of aerosols on cloud microphysics only parameter N_0 is changed. However, the slope parameter determines the relationship between concentration of smaller and larger CCN, so concentration of nucleated droplets also depends on the slope parameter. The simulations of the third set are referred to as E3500-S-05, EN3500-S-05, E100-S-05 and EN100-S-05. Size distributions of CCN in the simulations are shown in **Figure 1**.

CCN concentrations in the simulations s are presented in **Table 2**. Although the difference between the total aerosol concentrations in cases of k=0.5 and 0.9 is not large, in case k=0.5 the CCN size distribution contains more large CCN and fewer small CCN. These size distributions were assumed within the lower 2-km layer. Above this level, the CCN concentration in each mass bin was decreased exponentially with height. Above 8 km, the CCN concentration was set constant.

4. Results of simulations

4.1 Vertical profiles of supersaturation near cloud base

The model calculates supersaturation at the model grid points which typically do not exactly coincide with the cloud base level where supersaturation S_w =0. We consider the first level where $S_w \geq 0$ as the cloud base. Since the supersaturation maximum is reached not far from the cloud base level, especially for high AP concentration cases (Pinsky et al. 2012), we attribute the

values of $S_{\max}$ to this level. Correspondingly, the difference between the droplet concentrations in NA and ST is also attributed to this level. **Figure 2** shows vertical profiles of supersaturation calculated in ST and NA simulations in the atmospheric columns where the velocity at cloud base was equal to 1 ms^{-1}. It is natural that the values of $S_{\max}$ are larger in case of low CCN concentration as compared to high CCN concentration case. For goals of the present study, a more interesting finding is that the values of $S_{\max}$ calculated using NA are substantially larger than S_w calculated at model level associated to the cloud base in ST. The difference between NA and ST in the supersaturation values leads to a substantial difference in the droplet concentrations, especially in cases of high CCN concentration. Calculation of $S_{\max}$ at cloud base changes the vertical profile of supersaturation above it. While in ST supersaturation changes only slightly or even increase with height within 100-200 m above cloud base, in NA supersaturation decreases within this layer above the supersaturation maximum in agreement with the theory (Rogers and Yau, 1989, Pinsky et al, 2012, 2013).

To justify the values of supersaturation and droplet concentration obtained in NA, benchmark simulations using a parcel model were performed. The parcel model describes AP and drops using drop size distribution defined on a mass grid containing 2000 mass bins (Pinsky et al, 2002). It calculates growth of AP and droplets by solving the equation for diffusional growth written in the most general form without using parameterization of droplet nucleation. Time step used for solving the diffusional growth equation was 0.001 s. The model was used earlier for developing lookup tables relating parameters of AP and vertical velocity to droplet concentration (Segal and Khain, 2006). Simulations with the parcel model were performed for the same vertical velocity at cloud base, temperature and CCN distributions as in the HUCM simulations. As can be seen from Fig. 2, the values of supersaturation and droplet concentration calculated using NA are

much closer to those calculated using the parcel model as compared to the values calculated using ST.

The model level associated with the cloud base (where $S_w \geq 0$) is slightly higher than the lifting condensation level (LCL), where $S_w = 0$. At the same time, the calculations performed according to Pinsky et al. (2012) show that the level where $S_w = S_{\max}$ is located from about 20 m (for high CCN concentration) to about 60 m (for low CCM concentration) higher than the LCL. The estimations show, therefore, that the level where $S_w = S_{\max}$ is quite close to the model cloud base level. Accordingly, the droplet concentration determined at $S_w = S_{\max}$ is assigned to the corresponding grid point at the model cloud base.

4.2 High CCN concentration

In this section we compare the results for three pairs of simulations of clouds were developing in a highly polluted atmosphere. **Figure 3** shows the fields of droplet concentration N_d at the developing stage of the cloud evolution in E3500-S-0.5 (a), EN3500-S-0.5 (b), E3500-S (c) and EN3500-S (d). The maximum N_d in NA is reached at cloud base, which makes the cloud base well pronounced. The difference between droplet concentrations in ST and NA experiments decreases with height. The highest droplet concentration is reached in simulations where the CCN activation spectrum was characterized by the slope parameter k=0.5. This can be attributed to the fact that at k=0.5 the aerosol spectrum contains more CCN which are activated at cloud base than at k=0.9.

255 Vertical profiles of the maximum values of droplet concentration and of cloud water content
256 (CWC) averaged over time periods of storm development (a-b) and over the mature stage (c,d) are
257 presented in **Figure 4.**

258 In NA the N_d maximum is reached near cloud base and the droplet concentration decreases
259 with height. This behavior of $N_d(z)$ is more realistic than in ST, where N_d increases with height
260 up to an altitudes 2- 4 km, depending on the stage of storm evolution. This increase in the N_d in
261 ST is caused by in-cloud activation of mid-size CCN which were not activated at cloud base in the
262 standard approach. In NA, these CCN were activated at cloud base. There is, therefore, a negative
263 feedback in the supersaturation-droplet concentration relationship: an underestimation of
264 supersaturation at low levels in the ST simulations leads to the underestimation of droplet
265 concentration and to the corresponding increase in supersaturation at comparatively small
266 distances above cloud base. These results indicate that in models where droplet nucleation is
267 calculated only at cloud base, the correct calculation of $S_{\max}$ at cloud base is *strictly necessary to*
268 *obtain reasonable values of* N_d in clouds.

269 At height of about 4-5 kilometers, droplet concentrations in ST and NA become nearly
270 similar. Figs. 4a,c show also that N_d is very sensitive to the slope parameter of the CCN
271 activation spectrum. The maximum N_d reached at cloud base is about $1100\,cm^{-3}$ in EN3500-S-
272 05 (k=0.5) as compared to ~$550\,cm^{-3}$ in EN3500-S (k=0.9). This difference is caused by the fact
273 that in case k=0.5 the concentration of CCN with sizes exceeding ~$0.015\,\mu m$ (which are activated
274 at cloud base) is larger than in case k=0.9 (see Fig.1).

275 The effect of the *smallest* CCN on N_d (and on entire ice microphysical structure) becomes
276 very important above 6 km. In simulations containing the smallest CCN, these CCN are activated

277 producing new small droplets at heights of around 6.5- 8 km. The increase in N_d is shown in Fig.
278 4a,c by red arrows. These smallest CCN are not activated at cloud base even in NA (where $S_{\max}$
279 is larger than S_w in ST). This in-cloud nucleation is caused by an increase in supersaturation at
280 these levels due to a decrease in CWC (Fig. 4b,d) and an increase in vertical velocity (not shown).
281 The increase in N_d by activation at high levels and its effect on concentration of ice crystals in
282 cloud anvils of deep convective clouds was also reported by Khain et al. (2012).

283 Since the slope parameter determines concentration both of larger CCN and of smallest
284 CCN, the slope parameter also affects the concentration of droplets nucleated at high levels.

285 Vertical profiles of CWC (Figs. 4b,d) are typical of deep convective clouds developing in
286 the highly polluted environment: CWC is large and has maximum at about 5 km, i.e. at quite high
287 altitude.

288 **Figure 5a** shows the vertical profiles of maximum concentration of plate crystals (in HUCM
289 homogeneous freezing leads to formation of plates) averaged over the mature stage of cloud
290 evolution (from 4860 to 5460s). The number concentration of ice crystals in E3500 and EN3500
291 (in which there are no the smallest CCN in the initial CCN spectrum) is by factor of 5 lower than
292 in simulations with the CCN spectra containing the smallest CCN. The results show that ice
293 crystal concentration in NA is higher only slightly than in ST. Thus *the concentration of ice*
294 *crystals in cloud anvils is determined to a large extent by the concentration of smallest CCN in the*
295 *CCN spectra and is substantially less sensitive to larger CCN, which are activated at cloud base*.
296 Figure 5b shows that this conclusion is valid for the entire period of the simulation. In agreement
297 with Fig. 4c, the concentration of plates increased when NA was used (**Fig. 5b**). The comparative
298 contribution of the smallest CCN and CCN additionally activated at the cloud base in NA (as
299 compared to ST) are shown in Fig. 5b by arrows.

300 **Figure 6** shows the vertical profiles of time averaged maximum mass contents of ice
301 crystals, snow, graupel and hail+freezing drops at the storm mature stage. The maximum
302 difference between ice crystal mass contents takes place at ~10-11 km, where ice crystals are
303 caused by homogeneous freezing.

304 The most pronounced effect of NA is an increase in the accretion rate. In agreement with
305 results of simulations of aerosol effects on ice microstructure of deep convective clouds (Khain
306 2009; Tao et al. 2012; Khain et al. 2016), the intensification of riming leads to a decrease in the
307 snow mass content and to an increase in the mass contents of graupel (Fig.6b-c). The existence of
308 the smallest CCN concentration leads to further decrease in the snow mass content and to the
309 increase in the graupel mass content. This smallest CCN lead to higher supercooled droplet
310 concentration and to an increase in the liquid mass available for riming (Fig. 4d,e).

311

312 **4.3. Low CCN concentration**

313 In this section we compare the results for three pairs of simulations: a) E100 and EN100, b)
314 E100-S and EN100-S, and c) E100-S-0.5 and EN100-S-0.5 in which clouds were developed in the
315 atmosphere with low CCN concentration. After the first 35 min of cloud evolution, the cloud base
316 is located at 700-800 m altitude and T=16.8℃ at this level.

317

318 The fields of droplet concentration N_d in different simulations at the developing stage of the
319 cloud evolution are shown in **Figure 7**. The maximum N_d in a NA is reached at cloud base, which
320 makes the cloud base well pronounced. The difference in droplet concentrations between ST and
321 NA simulations decreases with height**.** Although the difference is N_d between NA and ST is very

pronounced, the absolute difference is not large (about $20\,cm^{-3}$). This low N_d determines a typical maritime microphysical structure of clouds in both NA and ST cases.

Figure 8 shows vertical profiles of the maximum values of droplet concentration and cloud water content (CWC) averaged over the time period of 3420-4020s (mature stage). One can see a dramatic difference in the profiles of droplet concentration and between CWC values of at low CCN concentration as compared to high CCN concentration (Fig. 4). At low CCN concentration, droplet collisions are efficient and droplet concentration decreases with height much faster than in polluted air. As a result, the CWC maximum at low CCN concentration is located at the height of 2 km as compared to 5 km in case of high CCN concentration. These differences determine the huge difference in the ice microphysics.

Fig. 8 shows that both the droplet concentration and CWC are larger in NA as compared to ST. The main differences between droplet concentrations near cloud base are, however, determined by the difference in the slope parameter value: at k=0.5 there are more CCN of sizes exceeding $0.015\,\mu m$ than at k=0.9 (Fig. 1).These CCN are activated at cloud base leading to higher concentration in simulations with k=0.5, especially when NA was applied.

Efficient collisions (seen by the sharp decrease in the CWC above z=2 km) and rain fall decrease the droplet concentration. As a result, the supersaturation increases and leads to in-cloud nucleation and an increase in the droplet concentration already at distances of a few hundred meters above the cloud base. However, since the concentration of CCN is low, the amount of new nucleated droplets in the simulations was only about 5-10 cm^{-3}. The second layer of intense in-cloud nucleation caused by activation of the smallest CCN is seen within the altitude layer from 4 km to 8 km. The difference in droplet concentration within this layer is fully related to the

existence/absence of smallest CCN in the CCN size spectrum. The differences between droplet concentration in ST and NA simulations are not significant at these levels.

This result agrees with the case of high CCN concentration when droplet concentration at higher levels is to a large extent determined by the smallest CCN in the droplet spectrum.

Figure 9 presents the vertical profiles of maximum mass contents of ice crystals, snow, graupel and hail + freezing drops at the mature stage of cloud evolution. Comparison with Fig. 6 shows that with the exception of snow, the mass contents of different ice hydrometeors at low CCN concentration are substantially lower than at high CCN concentration. The main reason for such difference is lower CWC at low CCN concentration that leads to less intense riming and, consequently to slow growth of ice particles.

Fig. 9 shows that the profiles of ice hydrometeors in NA and ST are similar. It means that the ice microphysics is to a large extent determined by the mass of supercooled droplets at high levels which in turn is determined by the *smallest* CCN in the CCN size spectrum. The effects of the smallest CCN and the shape of CCN size spectra on droplet concentration and the concentration on ice microphysics are much stronger than the effect of additional droplets nucleating at cloud base in the NA. The reason for this effect was explained above.

The increase in the concentration of the smallest CCN and in droplet concentration leads to an increase in the ice crystals mass content occurring about the level of homogeneous freezing (Fig.9a).

The mass content of snow decreases with the increase in the smallest CCN concentration, because intensification of riming of snow leads to its conversion to graupel (Fig. 9b). Consequently, the graupel mass content increases (Fig. 9c). As regards to mass content of hail, the increase in the smallest CCN concentration leads to a decrease in the hail content above 6 km

and to its increase below this level (Fig. 9d). The higher hail mass content above 6 km layer in the absence of smallest CCN is likely related to the fact that the low droplet concentration leads to formation of raindrops in high concentration. Although these raindrops are of comparatively small size, the total raindrop mass content is larger than that in case of higher drop concentration. These raindrops rapidly freeze above the freezing level producing hail (actually frozen drops) with total mass larger than at high CCN concentration. This effect is discussed by Ilotoviz et al. (2016) in detail. In HUCM, frozen raindrops are assigned to the hail category due to their high density. If hail is defined as particles with sizes exceeding 1 cm, the amount of hail at low CCN concentration would be negligible.

Higher hail mass content below 6 km in the presence of the smallest CCN can be attributed to intense conversion of heavy rimed graupel to hail, as well as to more efficient hail growth by riming. Note that sizes of hail particles forming in a deep convective cloud developing in the polluted atmosphere are larger than hail forming in a cloud developing in clean air (Ilotoviz et al. 2016). Due to larger size, hail in the polluted case falls to the surface (Fig. 6d), while in clean air hail melts at 1.5 km in the absence of small CCN, and in vicinity of the surface if the CCN size spectrum contains the smallest CCN.

4.3 The impact on precipitation

Figure 10a shows the accumulated rain at surface in the polluted air . Accumulated rain is maximum in EN3500-S-0.5 where effect of smallest CCNs is combined with the effect of comparatively large amount of large CCN. This synergetic effect of the smallest and large CCN

388 is described by Khain et al. (2011). In most simulations, the masses of accumulated rain are
389 quite similar.

390 Comparison of Fig. 10a and Fig. 10 b shows that the accumulated rain at low aerosol
391 concentration is lower than at high CCN concentration, which is in agreement with many
392 previous studies. Accumulated rain in NA was found to be quite close to that in ST. The main
393 difference in the values of accumulated rain at low CCN concentration is caused by effects of
394 smallest aerosols increasing the mass of precipitating ice particles .

395 Amount of hail at the surface in polluted air (**Figure 10c**) is substantially larger than in
396 clean air (**Figure 10d**) due to lower sizes and faster melting of hail particles if CCN
397 concentration is low. The effect of AP on the size and amount of hail at the surface was
398 investigated by Ilotoviz et al. (2016) in detail.

399 Amount of hail at the surface in polluted air is slightly higher in EN3500-S-0.5 as
400 compared to E3500-S-0.5 (**Figure 10c**). We attribute this effect to a higher rate 0of riming in
401 EN3500-S-0.5 due to a higher amount of supercoold water (Fig. 4b, d). There are no
402 significant differences in the other cases of polluted air.

403 The main factor determining the differences in the amount of hail falling to the surface at
404 low CCN concentration is the effect of smallest CCN. The increase in concentration of smallest
405 CCN leads to an increase in hail growth by riming.

406 As regards to the ratio of hail amounts in the experiments with smallest AP, earlier or later
407 intensification of convective cells (which is more or less random) may affect the ratio. Since
408 the mass of hail falling to the surface in clean air is very low, a larger computational area is
409 required to obtain reliable statistics.

410

5. Conclusions

Sensitivity of the microphysics of deep convective clouds to the concentration of aerosols and to the shape of aerosol size distribution is investigated using a new version of a 2D Spectral (bin) Microphysics Cloud Model (HUCM). A new component of the model is the calculation of maximum supersaturation at cloud base using the analytical expression derived by Pinsky et al. (2012). The cloud microphysical structure obtained using this expression is compared with that obtained with supersaturation calculated at model grid points.

The goal of the study was twofold: a) to test the effects of the improved calculation of supersaturation maximum near cloud base (NA (new approach) vs ST (standard approach)) at different aerosol loadings and b) to evaluate sensitivity of cloud microphysics to concentration and shape of size distribution of aerosol particles. In the simulations, shape of CCN size distributions was changed by changing the value of the slope parameter in the expression for activation spectrum (the values of k=0.5 and k=0.9 were used) and by adding the smallest CCN with radii below $0.015\,\mu m$.

The values of $S_{\max}$ near cloud base calculated by the theoretical analysis were found to be substantially larger than the supersaturation values calculated explicitly at model grid points associated with cloud base. The comparison of the values of supersaturation at cloud base and droplet concentration in the model simulations with the corresponding values calculated using a benchmark parcel model showed that NA simulates cloud base supersaturation and droplet concentration much more accurately than ST. Thus, *the first main conclusion* of the study is that the droplet concentration field in NA is substantially more realistic than in ST, with the maximum of droplet concentration in NA located near cloud base in agreement with classical results (Rogers

433 and Yau, 1989). The increased droplet concentration makes the cloud base more pronounced. The
434 improvement of the representation of the vertical profile of the droplet concentration is especially
435 significant in case of high CCN concentration, where utilization of S_{max} leads to a substantial
436 increase in the concentration of droplets near cloud base. Thus, even at 100-m vertical resolution,
437 it is necessary to use analytical expressions for S_{max} . At low CCN concentration, the improved
438 representation of droplet concentration above cloud base has a comparatively weak effect on cloud
439 microphysics. This result can be attributed to the fact that droplet concentration increases
440 relatively slightly if it is more accurately calculated since the available CCN concentration is low.
441 As a result, intense warm rain rapidly arises in both NA and ST.

442 The error in calculation of droplet concentration near cloud base in ST is compensated to a
443 significant extent by in-cloud nucleation above cloud base. Indeed, in NA droplet concentration
444 increases with height up to level of 4 km (Fig. 4a). The only reason of such increase is the in-cloud
445 nucleation of comparatively large CCN.

446 Models with microphysical schemes that do not describe in-cloud droplet nucleation should
447 include calculation of S_{max} at cloud base to avoid large errors in simulation of the microphysical
448 cloud structure.

449 *The second main conclusion* is high importance of the shape of CCN size distribution. Cloud
450 microphysics was found to be highly sensitive to the slope parameter of the CCN activation
451 spectra. The effect is comparable with the change in the total CCN concentration by the change in
452 the intercept parameter N_0. The utilization of k=0.5 instead of k=0.9 nearly doubled droplet

concentration near cloud base that leads to corresponding effects on cloud microphysics, in particular, to an increase in accumulated rain.

The third main conclusion is high sensitivity of ice microphysics to the existence of the smallest CCN in the CCN size spectrum. Both in cases of low and high CCN concentration, the differences in ice microphysics are determined to a large extent by *concentration of the smallest aerosols in the CCN spectra*. In cases of high CCN concentration, the effect of the smallest CCN in the NA becomes important above 5-6 km altitude where they are activated producing additional supercooled liquid droplets. The latter leads to the increase in the concentration of ice crystals above the level of homogeneous freezing by factor of about 5, to doubling of graupel mass maximum. The smallest CCN also influence hail size and mass content.

In case of low CCN concentration the smallest CCN also lead to an increase in the concentration and mass contents of ice crystals and to a significant increase of graupel and hail mass contents. Note that many probes of CCN measure concentration of CCN at supersaturations not exceeding 0.6%. In this case the concentration of the smallest CCN which remain non-activated at this supersaturation remains unknown. Such measurements do not provide necessary information for investigation of mixed-phase and ice microphysics.

Accumulated rain amount in case of high CCN concentration turned out to be higher than in case of low CCN concentration. This result was discussed by Khain (2009) and Ilotoviz et al.(2016) showing that formation of hail increases precipitation efficiency of mid-latitude storms.

Ice precipitation (calculated in mm of melted hail) at the surface is much lower than liquid precipitation. Nevertheless, hail precipitation at the surface in case of high CCN concentration is higher than in case of low CCN concentration by order of magnitude in agreement with results by

475 Khain et al. (2011) and Ilotoviz et al. (2016). This effect can be attributed by formation of larger
476 hail particles in case of high CCN concentration (high supercooled mass content). The large hail
477 particles reach the surface, while smaller hail forming in case of low CCN concentration melts
478 without reaching the surface.

479 The concentrations of drops and ice crystals are important parameters determining cloud
480 radiative properties. In this context, more accurate calculation of the concentrations using the NA
481 as well as taking into account the effects of smallest CCN should improve the accuracy of
482 evaluation of radiative cloud properties. The proposed approach of calculation of nucleation of
483 droplets at cloud base is simple in the utilization and computationally efficient. It can be used in
484 cloud-resolved models with different vertical grid spacing. The utilization of cruder vertical model
485 resolution may lead to larger errors in cases when droplet concentration at cloud base is calculated
486 using supersaturations calculated at model grid points.

487 *Acknowledgements*

488 The study is supported by the US Department of Energy Award DE_FOA-0000647 from the U.S.
489 Department of Energy Atmospheric System Research Program, by the Binational US-Israel
490 Science Foundation (grant 2010446), and by the Israel Science Foundation (grant 1393/14).

491

492 **Appendix. Derivation of an expression for the supersaturation maximum at cloud base**

493 Detailed description of the derivation of Eq. (1) is given in Pinsky et al. (2012). Below we present
494 only a short description. Assuming that near cloud base $S_w << 1$, the equation for supersaturation
495 can be written as:

$$\frac{dS_w}{dt} = A_1 \frac{dz}{dt} - A_2 \frac{dq_w}{dt} \qquad \text{(A1)}$$

where coefficients A_1 and A_2 are presented in T**able 1**; z is the height above cloud base and q_w is liquid water mixing ratio. The first term on the right-hand side of eq. (A1) describes an increase in supersaturation due to adiabatic air cooling during ascent, whereas the second term describes the supersaturation decrease caused by condensation of water vapor on droplets. Integration of equation (A1) leads to the equation of mass balance:

$$S_w = A_1 z - A_2 q_w + C_1 \qquad \text{(A2)}$$

where $C_1 = 0$ at cloud base. Assuming monodisperse DSD with droplets of radii r, the liquid water mixing ratio can be written as:

$$q_w = \frac{4}{3}\pi \frac{\rho_w}{\rho_a} N_d r^3 \qquad \text{(A3)}$$

where N_d is the droplet concentration. The equation for diffusional growth can be written is the form where the curvature term and the chemical term are omitted (Pinsky et al. 2012):

$$\frac{dr}{dt} = \frac{1}{Fr} S_w \qquad \text{(A4)}$$

The expression for coefficient F is presented in **Table 1**. CoefficientsA_1, A_2 and F slightly depend on temperature and can be assumed constant in the analysis. Using Eqs. (A2-A4), eq. (1) can be rewritten in the closed form as:

$$\frac{dS_w}{dz} = A_1 - \frac{1}{w} B_1 (A_2 N_d)^{2/3} (A_1 z - S_w)^{1/3} S_w \qquad \text{(A5)}$$

where $B_1 = \frac{3}{F}\left(\frac{4\pi}{3}\frac{\rho_w}{\rho_a}\right)^{2/3}$

Pinsky et al. (2012) showed that Eq. (A5) can be written in a non-dimensional form that results in an universal profile of supersaturation with height at given vertical velocity. The condition $\frac{dS_w}{dz} = 0$ applied to this equation allows to get solution in the form (1) for $S_{\max}$, as well as for the height of $S_{\max}$ over the cloud base. Pinsky et al. (2012, 2014) showed that (1) is valid for any size distributions of CCN.

References

Abdul-Razzak, H., and S. J. Ghan (2000), A parameterization of aerosol activation: 2. Multiple aerosol types, *J. Geophys. Res.*, *105*(D5), 6837, doi:10.1029/1999JD901161.

Abdul-Razzak, H., S. J. Ghan, and C. Rivera-Carpio (1998), A parameterization of aerosol activation: 1. Single aerosol type, *J. Geophys. Res.*, *103*(D6), 6123, doi:10.1029/97JD03735.

Benmoshe, N., M. Pinsky, A. Pokrovsky, and A. Khain, 2012: Turbulent effects on the microphysics and initiation of warm rain in deep convective clouds: 2-D simulations by a spectral mixed-phase microphysics cloud model. *J. Geophys. Res.*, **117**, D06220, doi:10.1029/2011JD016603.

Bedos, C., K. Suhre, and R. Rosset (1996), Adaptation of a cloud activation scheme to a spectral-chemical aerosol model, *Atmos. Res.*, *41*(3-4), 267–279, doi:10.1016/0169-8095(96)00014-2.

Bigg, E. K., 1953: The formation of atmospheric ice crystals by the freezing of droplets. Quart. J. Roy. Meteor. Soc., 79, 510–519, doi:10.1002/qj.49707934207.

Cohard, J.-M., J.-P. Pinty, and C. Bedos (1998), Extending Twomey's Analytical Estimate of Nucleated Cloud Droplet Concentrations from CCN Spectra, *J. Atmos. Sci.*, *55*(22), 3348–3357, doi:10.1175/1520-0469(1998)055<3348:ETSAEO>2.0.CO;2.

Fountoukis, C. (2005), Continued development of a cloud droplet formation parameterization for global climate models, *J. Geophys. Res.*, *110*(D11), D11212, doi:10.1029/2004JD005591.

552 Freud E., and D. Rosenfeld, 2012: Linear relation between convective cloud drop
553 number concentration and depth for rain initiation. *J. Geophys. Res*. **117**, D02207.

554 Ghan, S. J., C. C. Chung, and J. E. Penner (1993), A parameterization of cloud droplet
555 nucleation part I: single aerosol type, *Atmos. Res.*, *30*(4), 198–221, doi:10.1016/0169-
556 8095(93)90024-I.

557 Ghan, S. J., L. R. Leung, R. C. Easter, and H. Abdul-Razzak (1997), Prediction of cloud
558 droplet number in a general circulation model, *J. Geophys. Res.*, *102*(D18), 21777,
559 doi:10.1029/97JD01810.

560 Ghan, S. J., H. Abdul-Razzak, A. Nenes, Y. Ming, X. Liu, M. Ovchinnikov, B. Shipway,
561 N. Meskhidze, J. Xu, and X. Shi (2011), Droplet nucleation: Physically-based
562 parameterizations and comparative evaluation, *J. Adv. Model. Earth Syst.*, *3*(4), n/a–n/a,
563 doi:10.1029/2011MS000074.

564 Heymsfield A. J., A. Bansemer, G. Heymsfield and A.O. Fierro (2009), Microphysics of
565 maritime tropical convective updrafts at temperatures from -20 *oC to -60 oC, J. Atmos. Sci., 66,*
566 *3530-3565.*

567 Ilotoviz, E., A. Khain, N. Benmoshe, V. T. J. Phillips, and A. Ryzhkov, 2016: Effect of
568 aerosols on freezing drops, hail and precipitation in a mid-latitude storm. *J. Atmos. Sci.*, 73,
569 109-144, http://dx.doi.org/10.1175/JAS-D-14-0155.1.

570 Khain, A. P., 2009: Notes on state-of-the-art investigations of aerosol effects on
571 precipitation: A critical review. Environ.Res. Lett., 4, 015004, doi:10.1088/1748-
572 9326/4/1/015004.

573 Khain, A., M. Ovtchinnikov, M. Pinsky, A. Pokrovsky, and H. Krugliak (2000), Notes on
574 the state-of-the-art numerical modeling of cloud microphysics, *Atmos. Res.*, **55**(3-4), 159–224,
575 doi:10.1016/S0169-8095(00)00064-8.

576 Khain, A. P., Benmoshe, N. and A. Pokrovsky, 2008: Factors Determining the Impact of
577 Aerosols on Surface Precipitation from Clouds: An Attempt at Classification, J. Atmos. Sci.,
578 65(6), 1721–1748, doi:10.1175/2007JAS2515.1.

579 Khain, A.P., D. Rosenfeld, A. Pokrovsky, U. Blahak, and A. Ryzhkov (2011), The role of
580 CCN in precipitation and hail in a mid-latitude storm as seen in simulations using a spectral
581 (bin) microphysics model in a 2D dynamic frame, *Atmos. Res.*, *99*(1), 129–146,
582 doi:10.1016/j.atmosres.2010.09.015.

583 Khain, A.P., V. Phillips, N. Benmoshe, and a. Pokrovsky, 2012: The Role of Small Soluble
584 Aerosols in the Microphysics of Deep Clean Clouds, *J. Atmos. Sci.*, *69*(9), 2787–2807,
585 doi:10.1175/2011JAS3649.1.

586 Khain A.and B. Lynn And J. Shpund, 2016: High Resolution WRF Simulations of
587 Hurricane Irene: Sensitivity to Aerosols and Choice of Microphysical schemes. Atmos.
588 Research. 167, 1 January 2016, 129–145.

589 Khvorostyanov, V. I., and J. a. Curry (2006), Aerosol size spectra and CCN activity
590 spectra: Reconciling the lognormal, algebraic, and power laws, *J. Geophys. Res.*, *111*(D12),
591 D12202, doi:10.1029/2005JD006532.

592 Kogan Y.L. 1991: The simulation of a convective cloud in a 3-D model with explicit
593 microphysics. Part I: Model description and sensitivity experiments. *J. Atmos. Sci*., **48**,
594 1160–1189.

595 Meyers, M. P., P. J. DeMott, and W. R. Cotton, 1992: New primary ice-nucleation
596 parameterizations in an explicit cloud model. J. Appl. Meteor., **31**, 708–721.

597 Phillips, V. T. J., A. Pokrovsky, and A. Khain, 2007: The influence of time-dependent
598 melting on the dynamics and precipitation production in maritime and continental storm clouds.
599 J. Atmos. Sci., **64**, 338–359, doi:10.1175/JAS3832.1.

600 Phillips, V. T. J., A. Khain, N. Benmoshe, A. Ryzhkov, and E. Ilotovich, 2014:Theory of
601 time dependent freezing. Part I: Description of scheme for wet growth of hail. J. Atmos. Sci.,
602 **71**, 4527–4557, doi:10.1175/JAS-D-13-0375.1.

603 Phillips, V. T. J., A. Khain, N. Benmoshe, A. Ryzhkov, and E. Ilotovich, 2015: Theory of
604 timedependent freezing. Part II: Scheme for freezing raindrops and simulations by a cloud
605 model with spectral bin microphysics. J. Atmos. Sci., **72**, 262–286, doi:10.1175/JAS-D-13-
606 0376.1.

607 Pinsky, M., Khain, A. P.:2002 Effects of in-cloud nucleation and turbulence on droplet spectrum
608 formation in cumulus clouds. *Quart. J. Roy. Met. Soc*., 128, 1-33.

609 Pinsky M., I. Mazin, A. Korolev and A. Khain (2012), Analytical estimation of droplet
610 concentration at cloud base, *J. Geophys. Res*. **117**, D18211, 14 PP.

611 Pinsky M., I.P. Mazin, A. Korolev , and A. Khain, 2013:Supersaturation and diffusional
612 droplet growth in liquid clouds. J. Atmos. Sci. 70, 2778-2793

613 Pinsky M., I. Mazin, A. Korolev and A. Khain (2014) Supersaturation and diffusional
614 droplet growth in liquid clouds: Polydisperse spectra . J. Geophys Res. 2014, 119, 12872-
615 12887.

616 Pruppacher, H.R., Klett, J.D., 1997. Microphysics of Clouds and Precipitation. 2nd edn.
617 Oxford Press, 914 p.

618 Rogers R. R. and Yau M. K, 1989: A Short Course in Cloud Physics, Pergamon press.
619 293pp.

620 Rosenfeld, D., U. Lohmann, G. B. Raga, C. D. O'Dowd, M. Kulmala, S. Fuzzi, A.
621 Reissell, and M. O. Andreae (2008), Flood or drought: how do aerosols affect precipitation?,
622 *Science*, *321*(5894), 1309–13, doi:10.1126/science.1160606.

623 Rotunno, R., and J. Klemp (1985), On the Rotation and Propagation of Simulated
624 Supercell Thunderstorms, *J. Atmos. Sci.*, *42*(3), 271–292, doi:10.1175/1520-
625 0469(1985)042<0271:OTRAPO>2.0.CO;2.

626 Segal Y. and Khain, A. P., 2006: Dependence of droplet concentration on aerosol
627 conditions in different cloud types: application to droplet concentration parameterization of
628 aerosol conditions, J. Geophys. Res. Vol. 111, D15204, doi:10.1029/2005JD006561

629 Shipway, B. J., and S. J. Abel (2010), Analytical estimation of cloud droplet nucleation
630 based on an underlying aerosol population, *Atmos. Res.*, *96*(2-3), 344–355,
631 doi:10.1016/j.atmosres.2009.10.005.

632 Takahashi, T., Endoh, T., Wakahama, G., 1991. Vapor diffusional growth of free-falling snow
633 crystals between -3 and -23^{o}C. J. Meteorol. Soc. Jpn. 69, 15–30.

Tao W.-K., Jen-Ping Chen, Zhanqing Li, Chien Wang, Chidong Zhang (2012), Impact of Aerosols on Convective Clouds and Precipitation. *Reviews of Geophysics.* 50, Issue 2, June 2012 DOI: 10.1029/2011RG000369.

Vali, G., 1994: Freezing rate due to heterogeneous nucleation. J. Atmos. Sci., 51, 1843–1856, doi:10.1175/1520-0469(1994)051,1843:FRDTHN.2.0.CO;2.

Table 1. List of symbols

Symbol	Description	Units
A	$\frac{2\sigma_w}{\rho_w R_v T}$	m
A_1	$\frac{g}{R_a T}\left(\frac{L_w R_a}{c_p R_v T}-1\right)$	m^{-1}
A_2	$\frac{1}{q_v}+\frac{L_w^2}{c_p R_v T^2}$	-
B	$\frac{\nu_n \Phi_s \varepsilon_m M_w \rho_n}{M_n \rho_w}$	-
B_1	$\frac{3}{F}\left(\frac{4\pi\rho_w}{3\rho_a}\right)^{2/3}$	$m^2 s$
C_1	$1.058(FA_1/3)^{3/4}\left(\frac{3\rho_a}{4\pi\rho_w A_2}\right)^{1/2}$	$m^{9/4}\ s^{-3/4}$

c_p	specific heat capacity of moist air at constant pressure	J kg^{-1}K^{-1}
D	coefficient of water vapor diffusion in the air	m^2 s^{-1}
e		
e_w	saturation vapor pressure above the flat surface of water	N m^{-2}
g	acceleration of gravity	m s^{-2}
F	$\left(\frac{\rho_w L_w^2}{k_a R_v T^2} + \frac{\rho_w R_v T}{e_w(T) D}\right)$	m^{-2} s
K	parameter of activity spectra	
k_a	coefficient of air heat conductivity	J m^{-1}s^{-1}K^{-1}
L_w	latent heat for liquid water	J kg^{-1}
M_n	molecular weight of aerosol salt	kg mol^{-1}
M_w	molecular weight of water	kg mol^{-1}
N_d	concentration of liquid droplets	m^{-3}
N_0	parameter of activation spectra	
P	pressure of moist air	N m^{-2}
q_v	water vapor mixing ratio air)	$kg\ kg^{-1}$
q_w	liquid water mixing ratio	$kg\ kg^{-1}$
$r_{\max}$	drop radius at $z = z_{\max}$	m
		-
S_w	$S_w = e/e_w - 1$ supersaturation over water	-
$S_{\max}$	supersaturation maximum	-
T	absolute temperature	^{o}K
T_C	temperature at cloud base	^{o}C
w	vertical velocity	m s^{-1}
z	height over condensation level	m
$z_{\max}$	height of supersaturation maximum	m
ε_m	soluble fraction	-
ρ_a	density of air	kg m^{-3}
ρ_N	density of a dry aerosol particle	kg m^{-3}

ρ_w	density of liquid water	kg m^{-3}
σ_w	surface tension of water-air interface	Nm^{-1}
ν_n	van 't Hoff factor	-

646

647

648

649 **Table 2**. CCN concentrations in different experiments in the boundary layer

	High CCN concentration, cm^{-3}		Low CCN concentration, cm^{-3}	
Slope parameter	No smallest CCN	With smallest CCN	No smallest CCN	With smallest CCN
k=0.9	840	2930	33	214
k=0.5	1552	3140	53	152

650

651

652

653

654

655

656

657

Figures

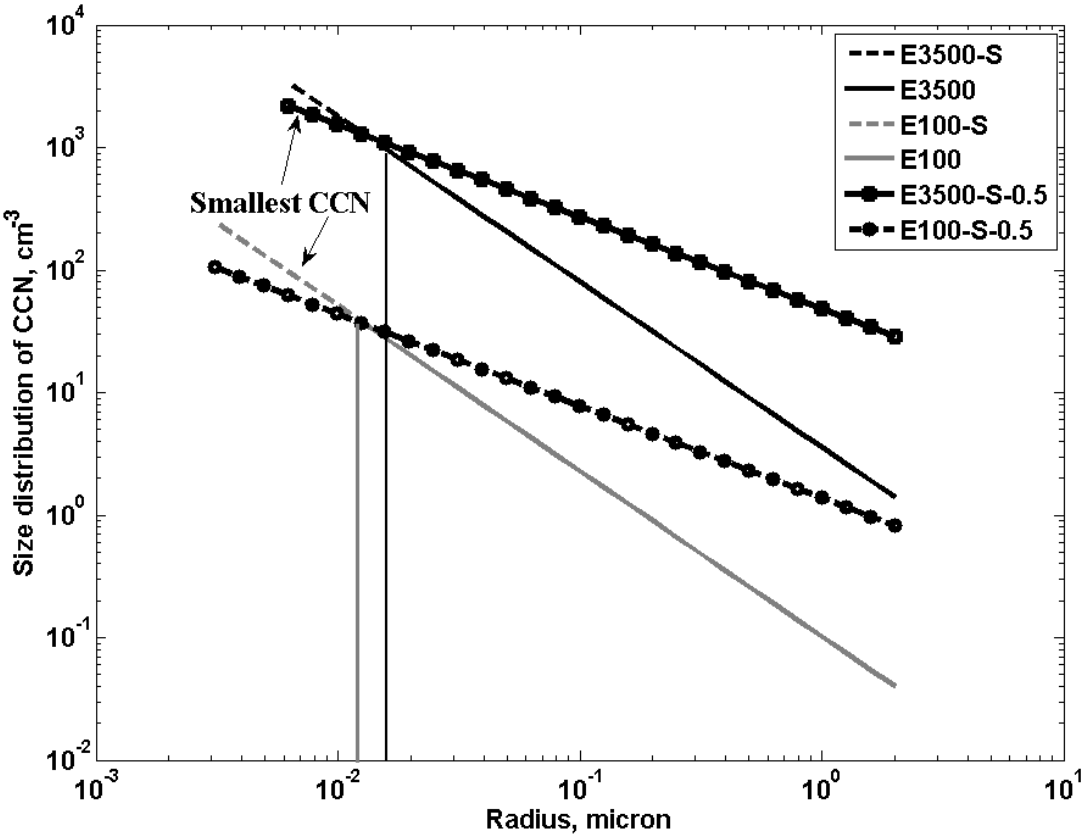

Figure 1. The initial size distributions of aerosols near the surface in different simulations.

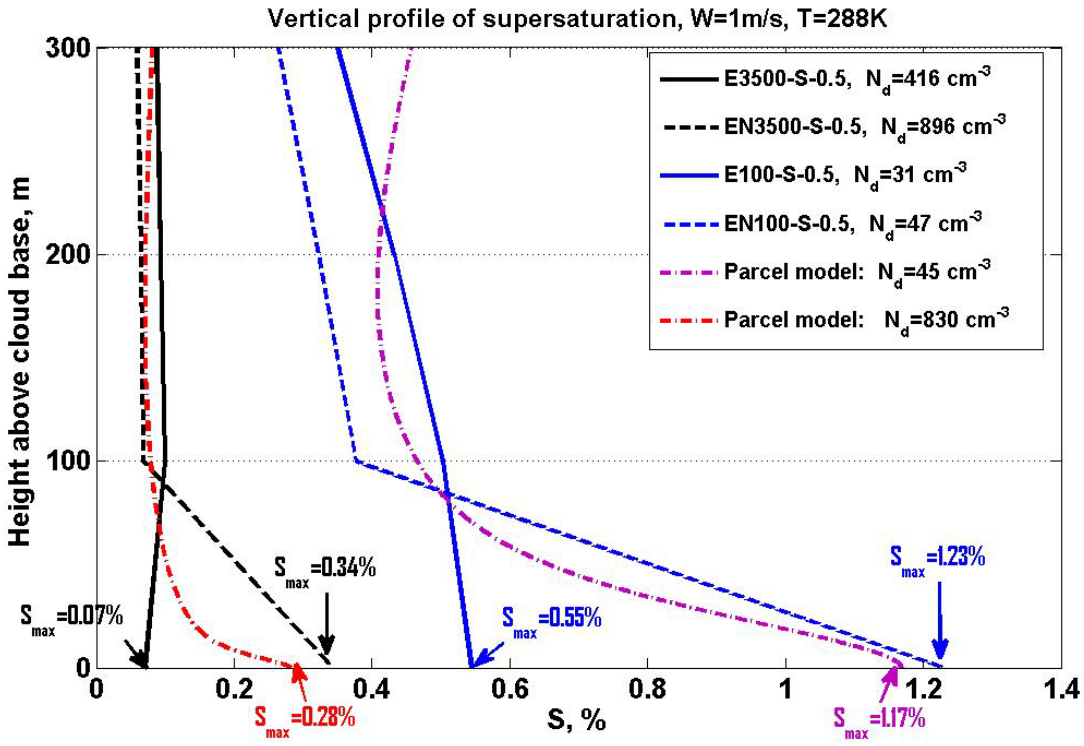

663

664 **Figure 2.** Examples of vertical profiles of the supersaturation above cloud base calculated using
665 HUCM and a benchmark parcel model. The columns with w close to 1 m/s at cloud base were
666 chosen for comparison. The values of S_{max} in HUCM were calculated according to *Pinsky et al.*
667 (2012). The values of droplets concentration calculated at cloud base in different simulations
668 are shown as well (see legend box).

669

670

671

672

673

674

675

676

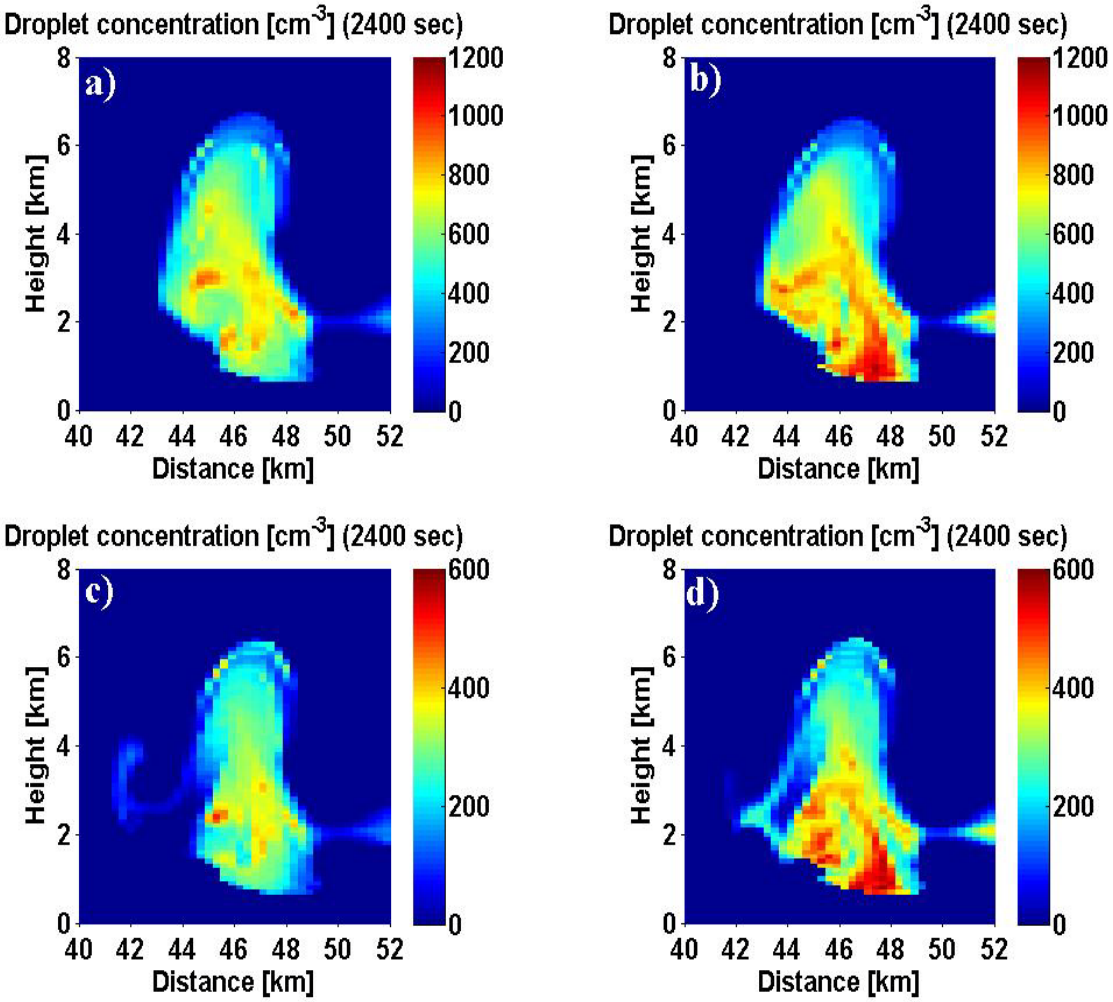

Figure 3. Field of droplet concentration at t=2400s in (a) E3500-S-0.5, (b) EN3500-S-0.5, (c) E3500-S and (d) EN3500-S.

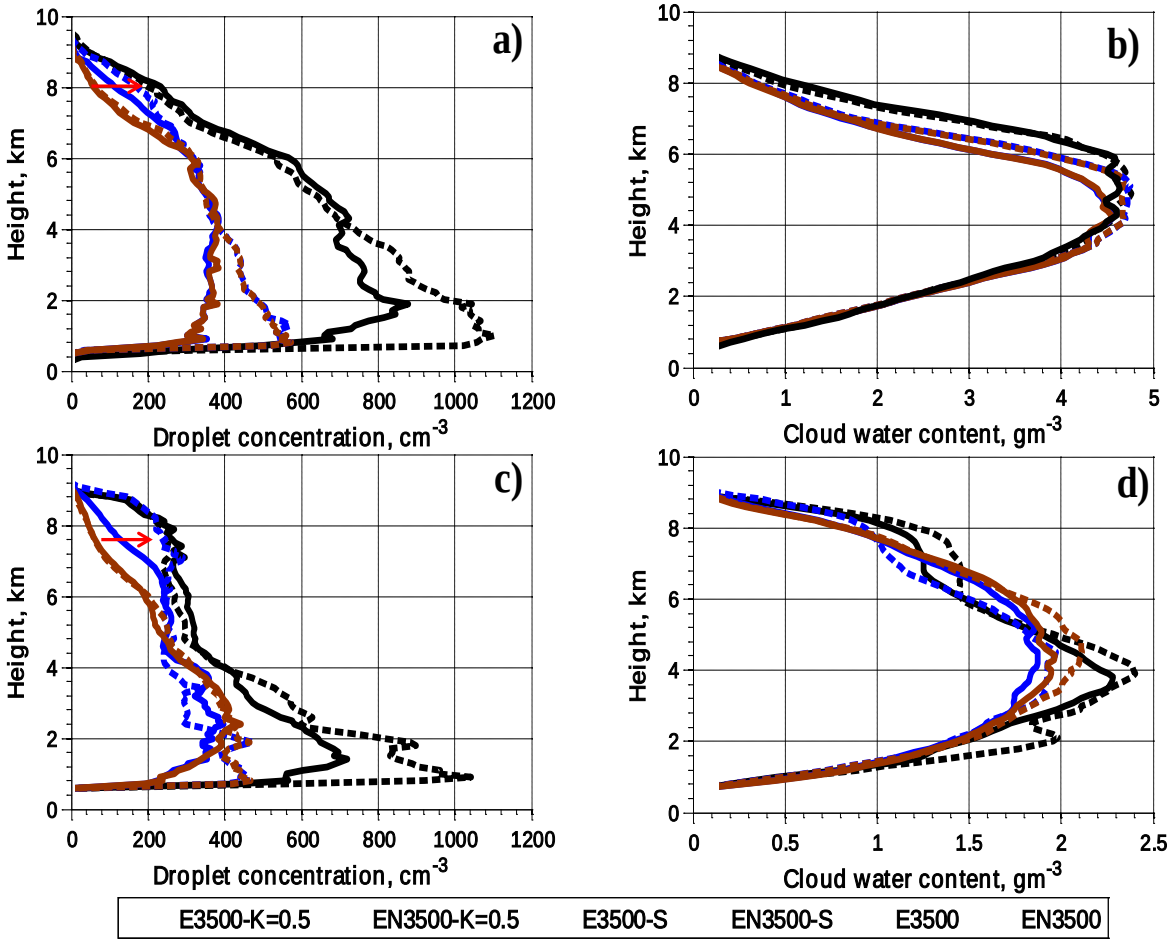

688

689

690 **Figure 4.** Vertical profiles of the maximum values of droplet concentration (a,d) and CWC(b, d)
691 in simulations with high CCN concentration. The profiles are obtained by averaging over the
692 time period of 2400-3000s (upper row) and over time period of 4860-5460s (bottom row). Panel
693 (c) shows a zoom of panel (b) for large CWC.

694

695

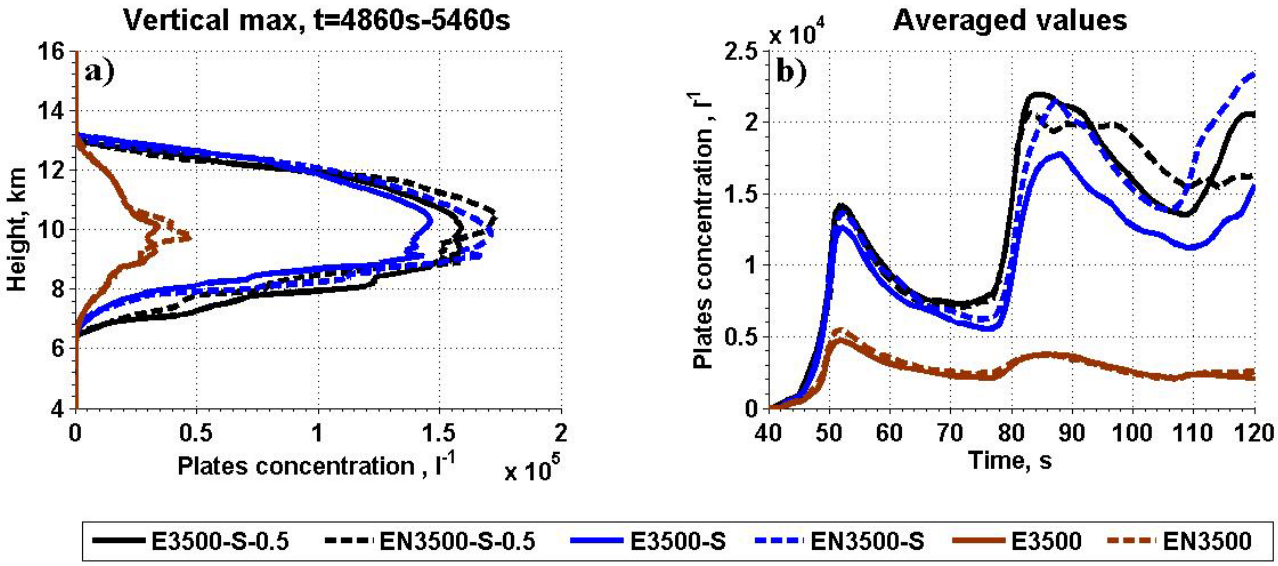

696

697

698

699

700 **Figure 5.** Vertical profiles of (a) maximum values of plates concentration and (b) time
701 dependencies of averaged plate concentration. The profiles are obtained by averaging over the
702 time period of 4860-5460s. The low and the upper arrows in the panel b show approximate
703 contribution of smallest CCN and the additional CCN activated in NA, respectively.

704

705

706

707

708

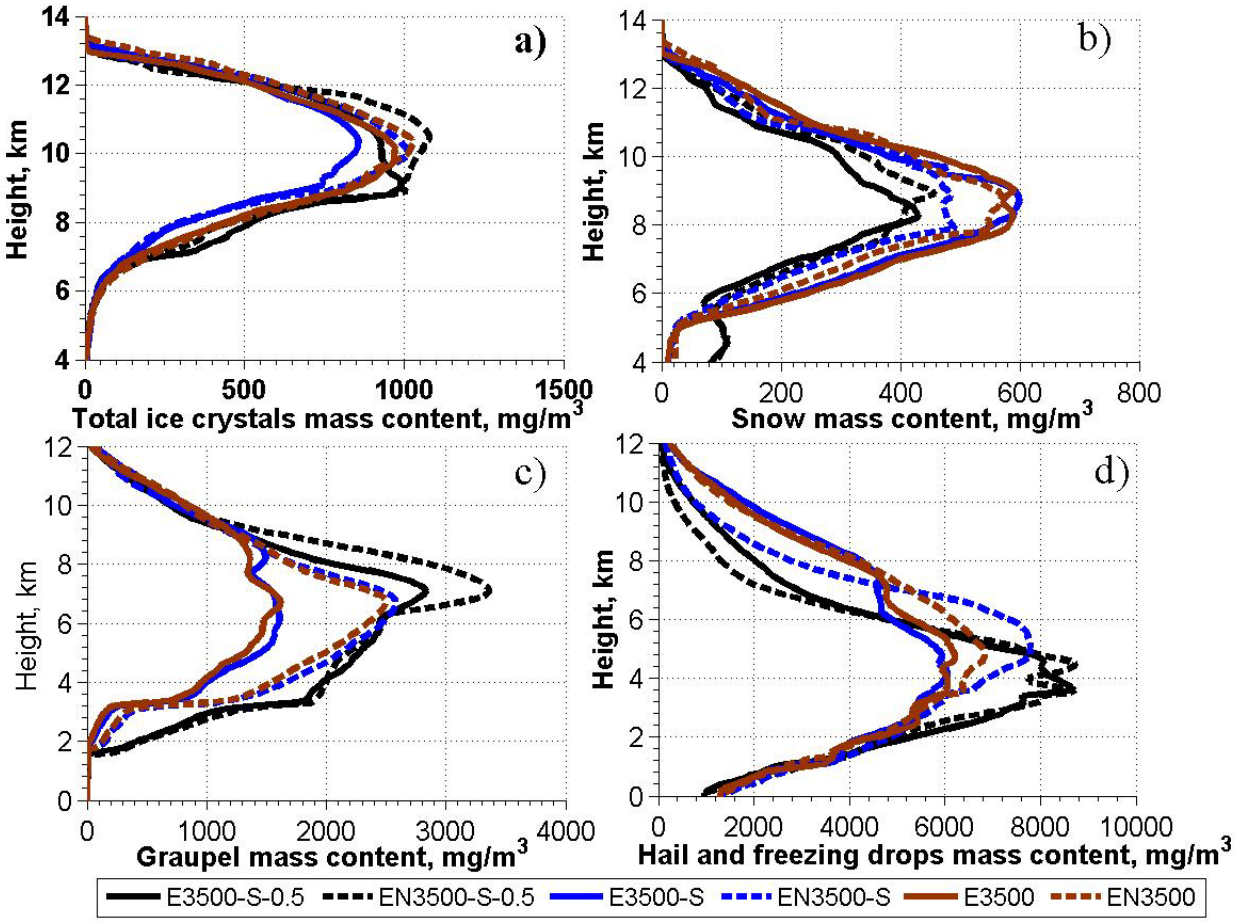

709

710

711 **Figure 6.** Vertical profiles of the maximum values of mass content: (a) total ice crystals, (b)
712 snow, (c) graupel and (d) total hail and freezing drops in simulations with high CCN
713 concentration. The profiles are obtained by averaging over the time period of 4860-5460s.

714

715

716

717

718

719

720

721

722

723

724

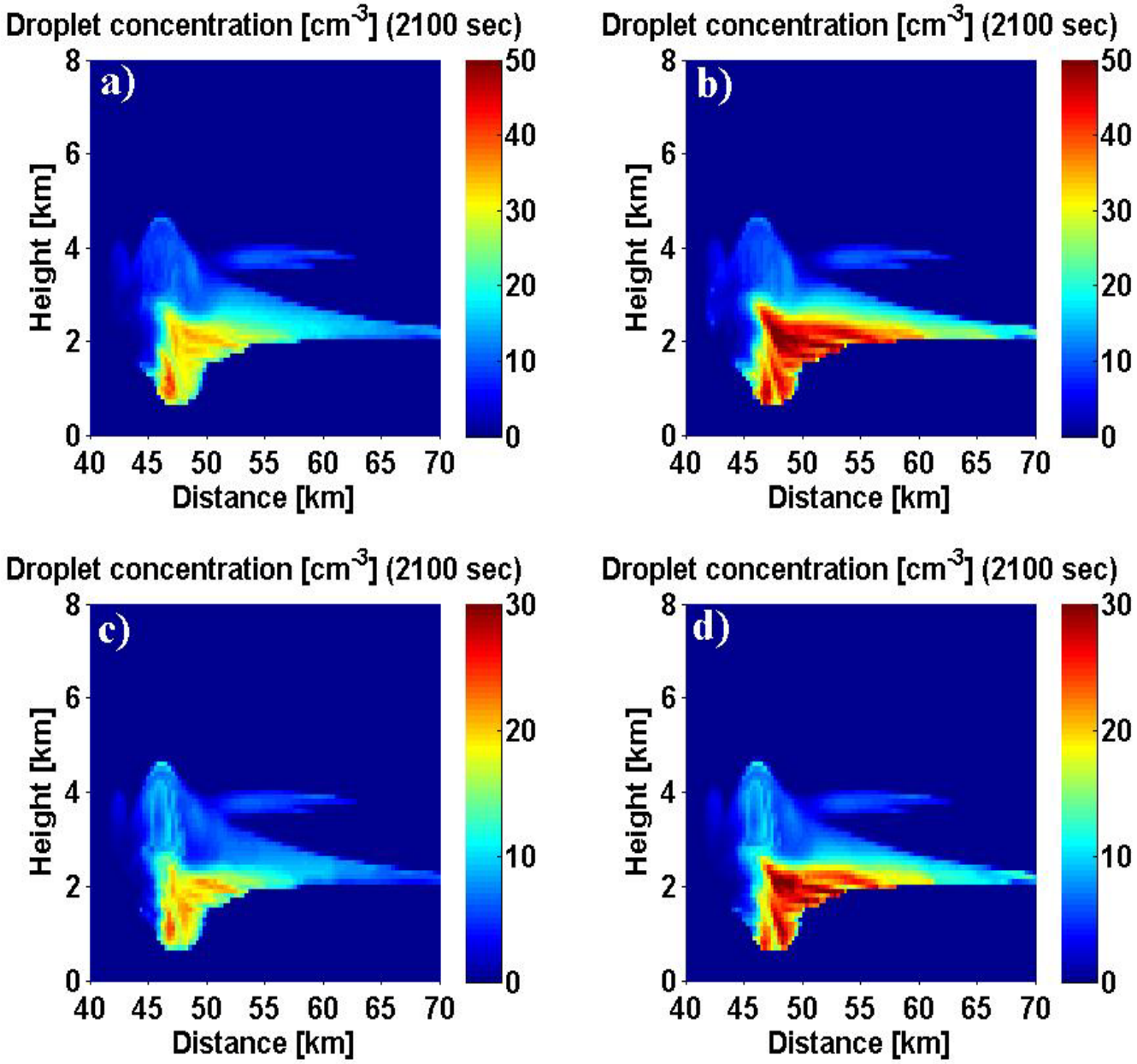

725

726

727

728 **Figure 7.** Fields of droplet concentration at t=2100s in (a) E100-S-0.5, (b) EN100-S-0.5, (c)
729 E100-S and (d) EN100-S simulations.

730

731

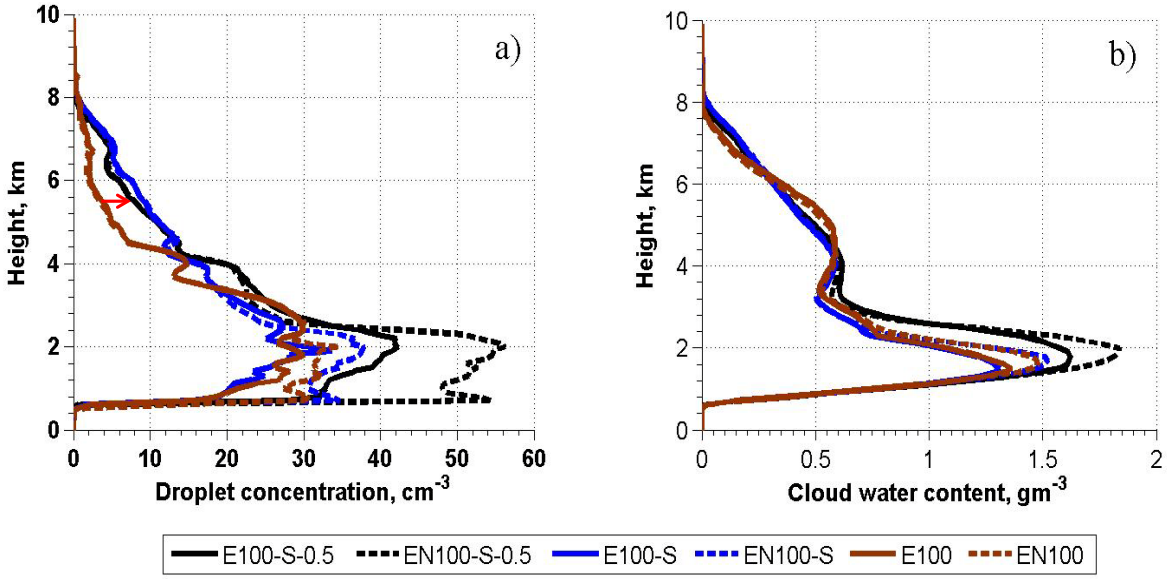

Figure 8. Vertical profiles of the maximum values of droplet concentration (a) and CWC (b) in simulations with low CCN concentration ($N_0 = 100\ cm^{-3}$). The profiles are obtained by averaging over the time period of 3420-4020s. Red arrow shows the increase in droplet concentration due to in-cloud nucleation in simulations with the CCN spectra containing small CCN.

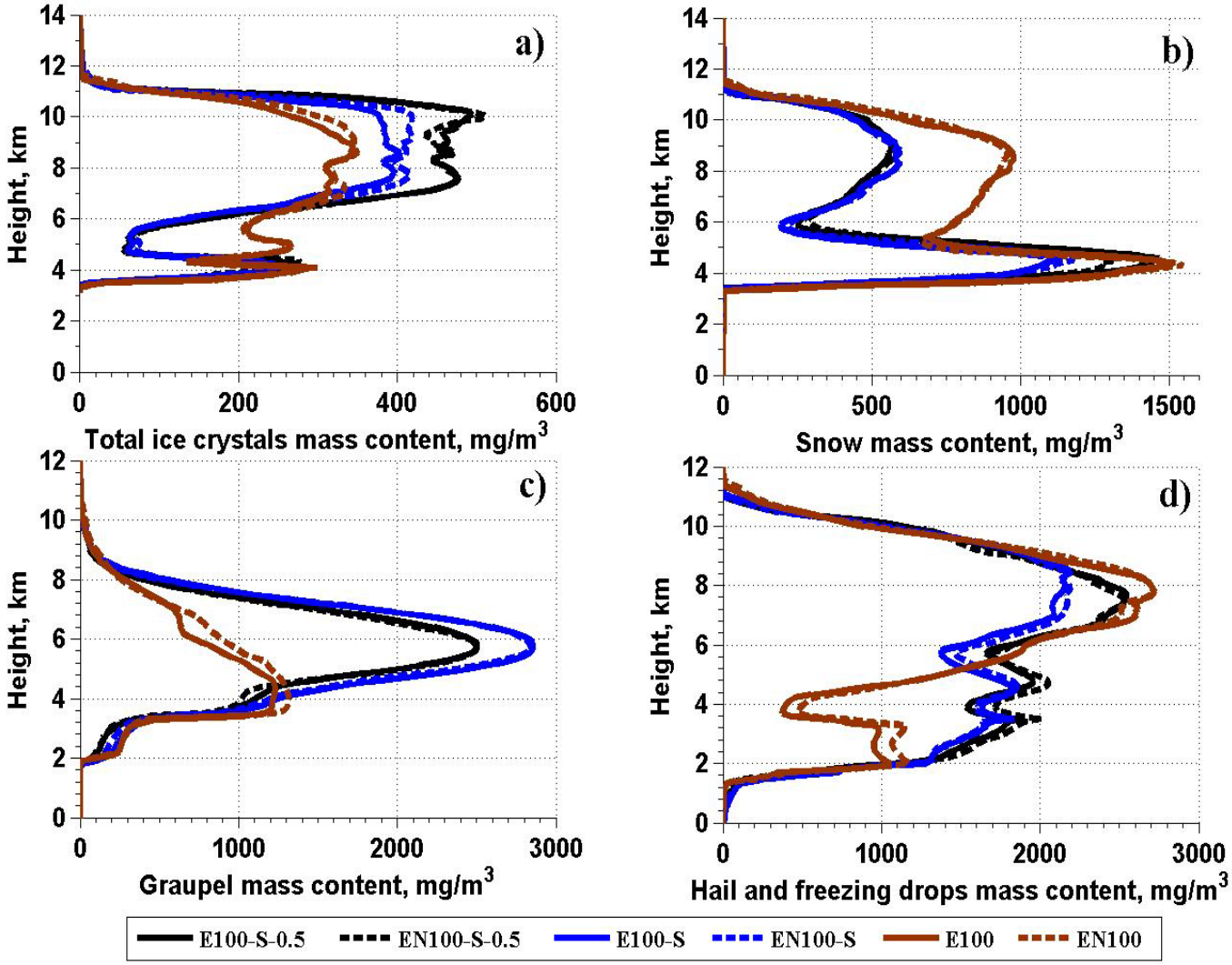

746

747

748 **Figure 9.** Vertical profiles of the maximum values of mass content: (a) total ice crystals, (b)
749 snow, (c) graupel and (d) total hail and freezing drops in the simulations with low CCN
750 concentration. The profiles are obtained by averaging over the time period of 3420-4020s.

751

752

753

754

755

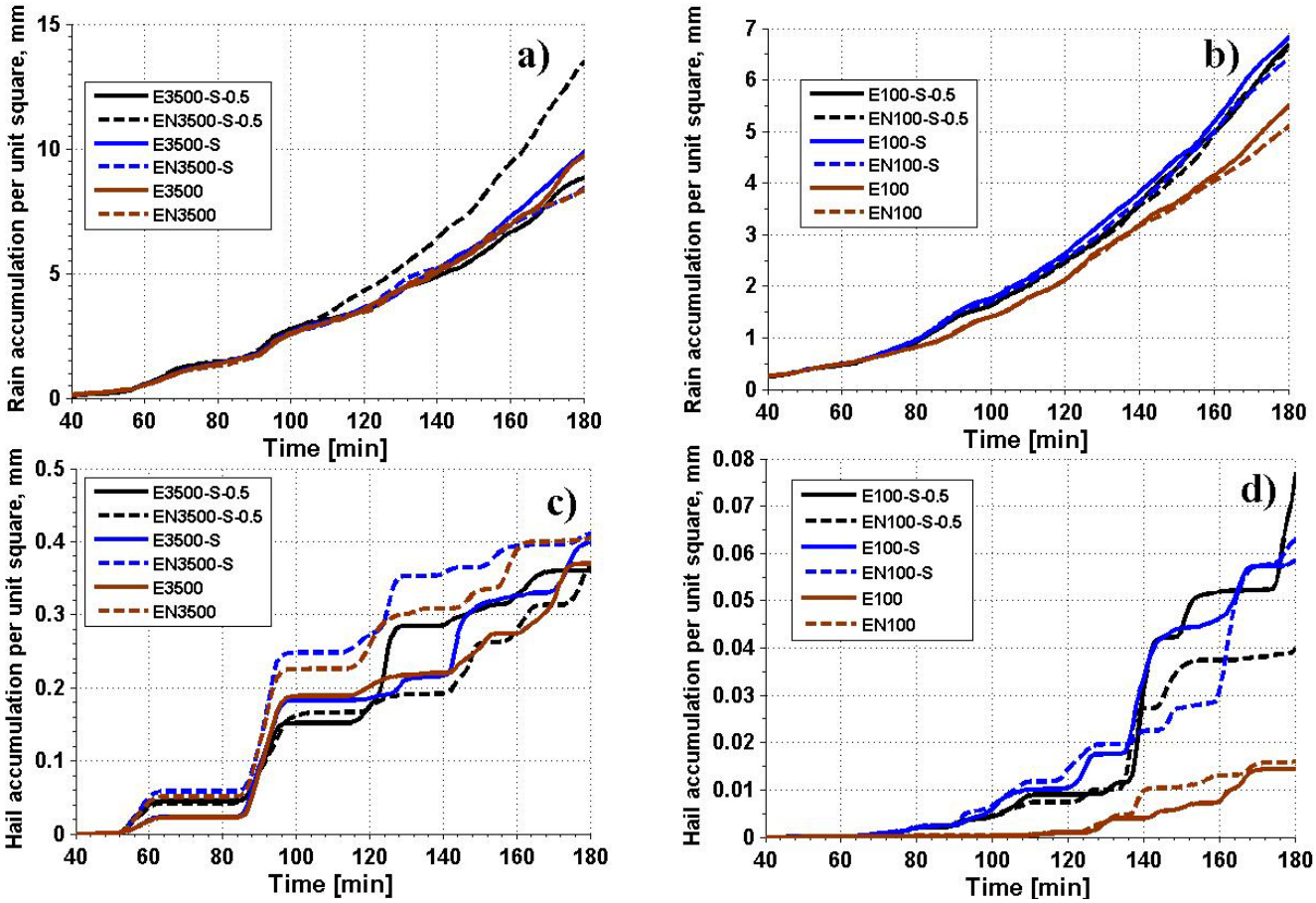

Figure 10. Time dependencies of (a) accumulated rain at surface for polluted and (b) for clean. Accumulated hail at the surface for polluted (c) and for clean (d) in different simulations in polluted cases.